ARTICLE IN PRESS

Available online at www.sciencedirect.com

SCIENCE DIRECT

ELSEVIER

Journal of Crystal Growth ▮ (▮▮▮▮) ▮▮▮–▮▮▮

JOURNAL OF CRYSTAL GROWTH

www.elsevier.com/locate/jcrysgro

Computational modeling of heat transport in a multi-zone high-pressure vertical electro-dynamic gradient CdZnTe furnace

M.D. Reed*, Cs. Szeles, S.E. Cameron

eV PRODUCTS, A Division of II–VI, Inc., Saxonburg, PA 16056, USA

Received 16 November 2004; received in revised form 1 December 2005; accepted 13 December 2005

Communicated by J.J. Derby

Abstract

The unsteady-state heat transport was computationally modeled in a multi-zone high-pressure vertical electro-dynamic gradient furnace using the Fluent software package. A 15,000-element, two-dimensional (2D) axisymmetric mesh and a 800,000-element 3D mesh were generated to model the solidification of CdZnTe during all phases of crystal growth. Temperature and flow fields were computed, and the effects of several materials properties and design parameters were quantified. The accuracy of the model was verified by experiment using both a graphite test fixture and a simulated load. Finally, the inclusion of a turbulent model to the simulation was shown to affect the gas phases, but not the molten CdZnTe.

PACS: 02.70.Fj; 47.27.−I; 81.05.Dz; 81.10.Fq; 83.20.Jp

Keywords: A1. Computer simulation; A1. Growth models; A2. Bridgman growth; B1. CdZnTe

1. Introduction

Computational fluid dynamics (CFD) is a useful tool for the exploration of physical phenomena in manufacturing processes that involve the transport of heat and fluid materials. The application of CFD to crystal growth is a natural one, due to the complicated nature of solidification phenomena, especially in multicomponent systems such as cadmium zinc telluride (CdZnTe) that are difficult to analyze in situ.

As a design tool, CFD is invaluable for exploration of physical phenomena, investigation of process sensitivities, and the virtual design of experiments and even entire crystal growth systems. Several researchers have explored the growth of CdZnTe by both horizontal and vertical Bridgman techniques [1,2], and described non-obvious phenomena using CFD modeling. Kuppurao and coworkers [3] investigated the effect of growth interruption schemes upon supercooling and interface stability in CdTe. Martinez-Tomas and Munoz [4] described the emissivity effect of pyrolytic carbon in quartz ampoule coatings for heat transport in vertical Bridgman growth. Yeckel et al. [5] analyzed the effect of crucible rotation upon CdZnTe growth, and found that an accelerated crucible rotation technique improves zinc segregation and also reduces constitutional supercooling. Without a robust CFD model, analysis of esoteric techniques such as these would be unavailable to the crystal growth engineer.

The system being modeled in this work was the Gen-3 High-pressure Electro-Dynamic Gradient Furnace system (hereafter referred to as the "HP-EDG" furnace) located at eV PRODUCTS. The Gen-3 HP-EDG furnace is a vertical melt growth system designed to produce large-diameter (140 mm) semi-insulating $Cd_{1-x}Zn_xTe$ ($x = 0.1$) ingots from a molten initial charge. High temperatures (in excess of 1100 °C) and high pressures (~100 atm) achieved through the employment of a thick-walled steel pressure vessel preclude direct observation, and limit data acquisition to power consumption, pressure, and temperature measurement. Furthermore, each experimental run is both time-consuming and costly. In such an environment, virtual

*Corresponding author. Tel.: +1 7243605878; fax: +1 7243524435.
E-mail address: mreed@ii-vi.com (M.D. Reed).

0022-0248/$ - see front matter © 2006 Published by Elsevier B.V.
doi:10.1016/j.jcrysgro.2005.12.103

testing of processes is an invaluable tool for design and optimization.

Before virtual furnaces can be modified and tested, underlying assumptions regarding the accuracy of the computational model must be proven correct by experimental testing and—where necessary—model revision and retesting. This paper describes work performed during model validation, and exploration of the importance of various physical parameters upon model predictions.

2. Model development

2.1. Description

The finite volume software package used to model the Gen-3 HP-EDG furnace was FLUENT 6.1, from the company of the same name. This program used a segregated Gauss–Seidel linear equation solver with an algebraic multigrid method to solve the equations of continuity, conservation of momentum, conservation of energy, and radiative flux over each volume of the computational mesh. Field values were taken at the center of the volume, and vector quantities were taken at the centroid of each face, interpolated by the first-order upwind scheme. For each iteration, the segregated approach solved for a single variable field (e.g., temperature) by considering all cells at the same time, then progressed to the next variable in the iteration. Although this approach was computationally more expensive, the opportunity to ultimately perform solidification modeling necessitated this choice.

For the segregated solver, the continuity equation used was in the differential form:

$$\frac{\partial \rho}{\partial t} + \nabla \cdot (\rho \vec{v}) = 0, \tag{1}$$

where $\vec{v}$ is the fluid velocity, and ρ is the density of the fluid, which for argon was calculated as an incompressible ideal gas. Conservation of momentum was given by the differential equation

$$\frac{\partial}{\partial t}(\rho \vec{v}) + \nabla \cdot (\rho \vec{v}\,\vec{v}) = -\nabla p + \nabla \cdot (\bar{\bar{\tau}}) + \rho \vec{g}, \tag{2}$$

where $\bar{\bar{\tau}}$ is the stress tensor

$$\bar{\bar{\tau}} = \mu \left[(\nabla \vec{v} + \nabla \vec{v}^{\,\mathrm{T}}) - \frac{2}{3} \nabla \cdot \vec{v} \bar{\bar{I}} \right] \tag{3}$$

and μ is the viscosity and $\bar{\bar{I}}$ the unit tensor [6].

The plans to eventually involve solidification modeling also determined the choice of the discrete ordinates (DO) radiation model, as the only model available to the segregated solver. In this model, two equations are solved in order to compute the temperature field. The first is the energy equation, in the form:

$$\frac{\partial}{\partial t}(\rho E) + \nabla \cdot (\vec{v}(\rho E + p)) = \nabla \cdot \left(k \nabla T - \sum_j h_j \vec{J}_j + (\bar{\bar{\tau}} \cdot \vec{v}) \right) + S_h, \tag{4}$$

where J is the diffusive flux of species j, E the kinetic energy $v^2/2$, S_k a generic source term (though unused in this treatment), and h the species enthalpy defined by

$$h = \int_{T_{\mathrm{ref}}}^{T} c_p \, \mathrm{d}T. \tag{5}$$

The second was the radiative transfer equation, which computed radiation as a field equation in the direction $\vec{s}$, in the method of a transport equation. Where $\vec{r}$ is the position, I the radiation intensity, a the absorption coefficient, and n the refractive index of the fluid medium, the radiative transfer equation in differential form becomes

$$\frac{\mathrm{d}I(\vec{r},\vec{s})}{\mathrm{d}s} + aI(\vec{r},\vec{s}) = an^2 \frac{\sigma T^4}{\pi}, \tag{6}$$

where scattering is much less important than absorption, as for graphite furnace components [4,6].

Radiation was modeled with the discrete ordinates radiation model with four azimuthal partitions in each angular direction and a 6×6 pixellation of each control angle. No turbulence models were used for the initial simulations, but a two-parameter $k-\varepsilon$ model was later used to evaluate the effect of turbulence on the heat and mass transport, and this will be described in a later section. Thermal equilibrium was defined as attained when the average temperature of the CdZnTe volume changed less than 0.05 °C over a 5-min time step, based upon the precision of a standard thermocouple. The operating and boundary conditions used corresponded to the standard operating conditions of the Gen-3 furnace, and are listed in Table 1. Temperatures are specified at the surface of the furnace heaters, as well as the so-called "far-field temperature"—T_{ff}—which was the surface temperature at the outside wall of the insulation assembly. Since neither the pressure vessel nor the support elements were modeled, this boundary condition represents a limiting value for the minimum system temperature, and was simply posited to be larger than the nominal pressure vessel wall temperature. The materials properties used are listed in Table 2.

The entire furnace was not modeled. The meshed volume was limited to the internal structures of the furnace, excluding the pressure vessel and the vapor space between the steel pressure vessel and the insulation assembly.

Table 1
Operating and boundary conditions used in validation simulations

Condition	Value
Pressure	Operating; ~100 atm
Gravity	−9.81 m/s^2
Zone 1 temperature	1120 °C
Zone 1 temperature	1120 °C
Zone 1 temperature	1120 °C
Zone 1 temperature	1120 °C
Zone 1 temperature	1110 °C
Far-field temperature	Variable (300–600 °C)

Table 2
Materials properties used in computations (from vendor product literature, unless noted)

Property	Material	Value	Units	References
Heat capacity	Lava	1420	J/kg K	[5]
	Graphite insulation	2420		
	Structural graphite	2420		
	Argon	520.64		[7]
Thermal conductivity	Lava	1.98	W/m K	[5]
	Graphite insulation	0.4		
	Structural graphite	18.59		
Density	Lava	2.38	g/cm^3	
	Graphite insulation	0.250		
	Structural graphite	2.250		
Absorption coefficient	Graphite insulation	20 000	m^{-1}	[4]
	Structural graphite	20 000		[4]
Viscosity	Argon, at STP	2.13×10^{-5}	kg/m s	[7]

Preliminary simulations were performed to test various meshing schemes, and the best results were obtained with a quadrilateral mesh, usually employed in a "pave" scheme. In this scheme, the quadrilaterals were not necessarily emplaced on a strict grid, but could instead be deformed and rotated to form a moiré pattern conformal with the area boundary. A two-dimensional (2D) axisymmetric mesh of 15,000 elements was generated (Fig. 1), and compared with the benchmark solution from a 202,000 element mesh. The location of the largest argon velocities was proximal to the fourth furnace zone in each case, and the radial distribution of velocity was within 2% of the baseline at this height. Furthermore, the temperature of the crucible was within 1 °C of the baseline throughout the crucible.

A three-dimensional (3D) mesh of 800,000 elements was also generated (Fig. 2), expressly for evaluating effects that were obviously not axisymmetric, such as heat transfer through support elements and thermocouples. No 3D mesh-independence simulations were performed upon this mesh, save for comparison with the 2D case, due to computational limits precluding a finer 3D mesh. All simulations were run on a Dell workstation with dual 3.1 GHz Pentium-4 processors. Each 2D time step required approximately 8 s to complete, and each 3D time step required between 30 s and 5 min, depending on the number of iterations required for convergence.

2.2. Experiment

Aside from uncertainties in the materials properties of this system, the far-field temperature was the primary unknown variable in the model, and was the focus of the first set of experiments. Once this value became known, in principle all mathematical aspects of the problem were fixed, and the model was "complete". The estimation of uncertainties in various materials properties would continue, but the mathematical model would be able to

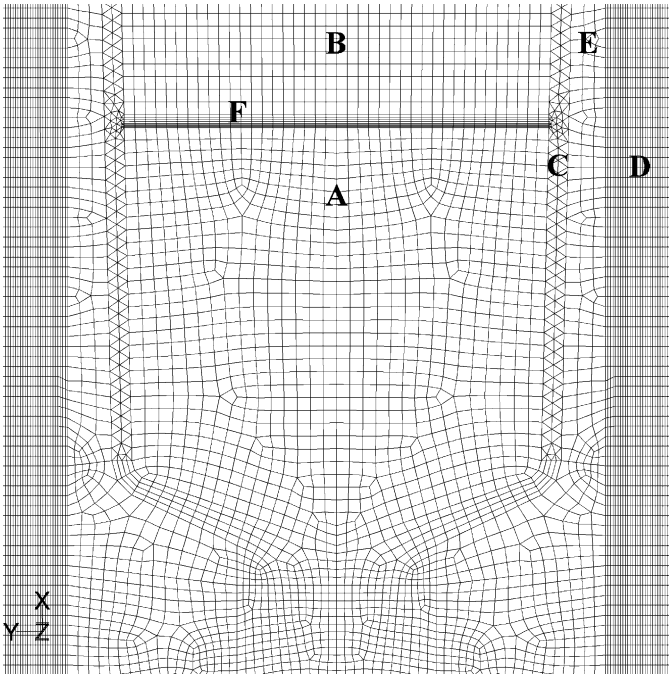

Fig. 1. Detailed view of 2D mesh section, illustrating melt (A), head vapor space (B), crucible (C), cylindrical graphite heaters, supports, and argon-filled vapor spaces (D), argon-filled internal space (E), and boundary layer at the melt–vapor interface (F).

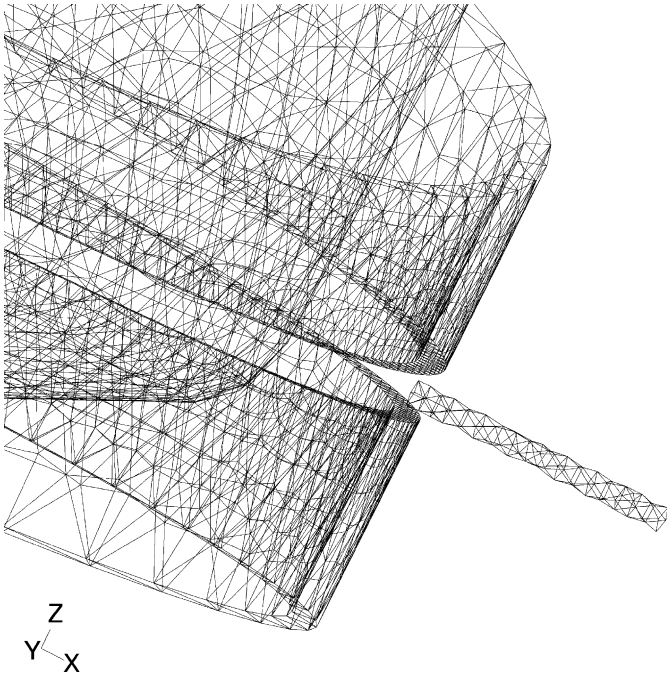

Fig. 2. Detailed view of 3D mesh segments, illustrating crucible, control thermocouple, and a heater section. Other furnace components have been rendered invisible in this view.

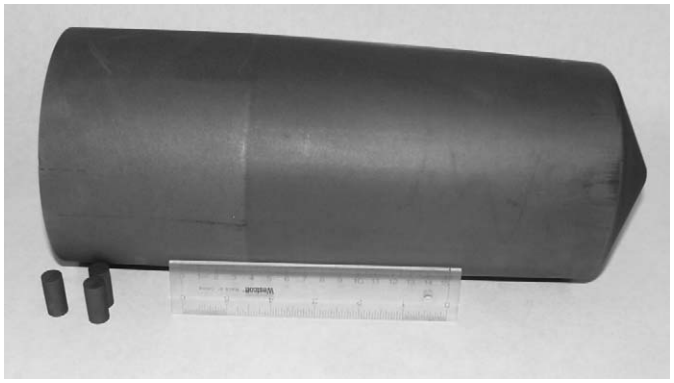

Fig. 3. Graphite insert. Graphite plugs, shown, were used to fill the thermocouple channel for non-centerline temperature measurements.

quantitatively estimate their effect, and often suggest upper and lower bounds for values.

Two classes of simulated growth experiments were conducted: one with a solid graphite body, and the second with a simulated load (described later). For the first, a solid graphite insert completely filled the crucible interior to create a solid block of graphite, with the exception of a centerline thermocouple channel (Fig. 3). Type R (Pt/Pt−13% Rh) thermocouples with a precision of $\pm 0.1\,^{\circ}$C were located at 76 and 203 mm from the bottom of the graphite block. This fixture created a simplified heat transfer scenario in which radiative and convective heat transfer would occur between furnace element and crucible, and only conductive heat transfer would occur within the crucible and inset graphite block. In this way, information regarding the thermal conductivity of the actual graphite material used could be obtained at high temperature using thermocouples at two different centerline heights. Furthermore, a baseline for the heat transferred by radiation and convection could be modeled for later comparison with simulated and real loads that have complicated interior flows that affect heat transfer. Finally, T_{ff} could be estimated based upon the temperature at the centerline.

For each experimental run, the furnace was pressurized over several hours and heated to the temperature of the homogenization step of the growth cycle, and maintained at those set point temperatures for 6 h to attain a steady state. After that, a quick shutdown cooling step was enabled, which immediately dropped the power supplied to each of the furnace zones to zero and began the process of unsteady-state multiple-mode (i.e. convective, conductive, and radiative) cooling to room temperature. Pressure, temperature, and power data were taken at 10-s intervals throughout the run.

2.3. Initial 2D simulations

The initial simulations of the Gen-3 furnace system used the 15,000-element 2D mesh to attempt to replicate the steady-state experimental results. These simulations were performed to test the mesh-independence of the system, to

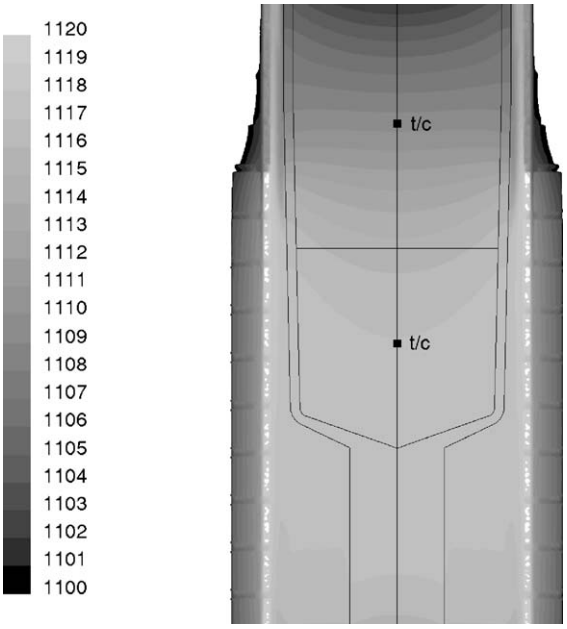

Fig. 4. Initial simulation of Gen-3 HP–EDG furnace with graphite insert. Top thermocouple temperature was measured experimentally to be 1114 °C; the simulation temperature is 1112 °C. The lower thermocouple temperature was measured to be 1124 °C; the simulation value was 1117 °C. Temperatures outside the scale bar are shown as white.

validate the physical properties of the materials, and to determine the sensitivity of the temperature field to various material parameters. Details of these simulations have previously been presented elsewhere [8]. Despite significant uncertainties in the materials parameters in the system ($\pm 50\%$ for the thermal conductivity of the graphite insulation, to name an extreme case), the equilibrium result yielded a temperature difference between experimental and computed values of less than 10°, uniformly under the experimental values (Fig. 4). This result was significantly more accurate than simulations reported previously [9].

These simulations demonstrated that the temperature field was relatively insensitive to variation in the far field temperature T_{ff}, with an average change of $<1\,^{\circ}$C centerline per 100 °C of far-field temperatures, for reasonable physical values of T_{ff}. By contrast, the centerline temperature was most sensitive to the thermal conductivity of the graphite insulation, varying 4 °C over the bounds of uncertainty. Other effects modeled included graphite thermal conductivity, transparency and viscosity of the argon at high pressure, density of the insulation and graphite insert, and absorption coefficient of the graphite. Also, the argon-filled thermocouple channel itself was meshed in two dimensions. Each of these cases resulted in a predicted variation of less than one degree at typical growth temperatures.

2.4. 3D simulation

While the 2D model replicated the experimental findings to within 10°, higher accuracy required the variation of the

Table 3
Temperature differences between heater elements and control thermocouples (°C)

Zone 1	−10
Zone 2	−10
Zone 3	−9
Zone 4	−10
Zone 5	−7

tested physical properties beyond the realm of credibility.Another possibility for the deviation from experiment seemed more likely: that the control thermocouples, which regulate the power supplied to the heating elements, were at a temperature lower than the surface of the elements themselves, which was the modeled parameter. In other words, the heating element surfaces were hotter than the set-point temperature of the control thermocouples, and should not be modeled as being at the control point values. The computational difficulty this engendered was that the thermocouple is necessarily a thin rod that makes the system longitudinally asymmetric. Therefore, not only did this require a 3D model, but also a model with enough resolution to model the thin thermocouple itself. The simulation conditions of the previous 2D model were transposed exactly; for instance, the surface temperatures of each heater zone were set to a given temperature during the calculation. Each 3D simulation required approximately a week of continuous computation to achieve steady-state. The results are shown in Table 3 and in Fig. 5, showing the temperature profile local to one of the control thermocouples.

As can be seen in Fig. 5, a significant temperature differential existed between the control thermocouple and the surface of the heating element. If the furnace control point were set to 1115 °C, for instance, the surface of the heater would actually have been at 1125 °C in order for the control thermocouple to read 1115 °C. The heater surfaces were increased by the differential amounts listed in Table 2, and then the simulation was permitted to converge. It is important to note that this process analytically replicated the actual control process of the furnace, in that the heater temperature was increased until the thermocouple set point was reached.

The resultant temperature profile exactly described the experimental temperature gradient between the two measurement thermocouples inside the graphite blocks, and predicted the absolute temperatures of the measurement thermocouples to within 2 °C. The 2D model replicated these results, as expected, and is shown in Fig. 6.

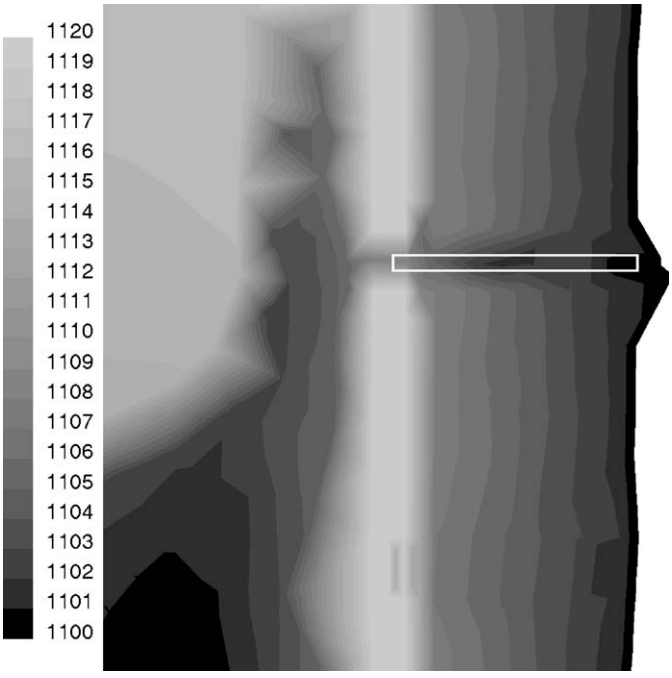

Fig. 5. Close-up view of temperature distribution in the region of the control thermocouple, which is superimposed in white. Low resolution is due to the coarseness of the 800,000-element 3D mesh employed.

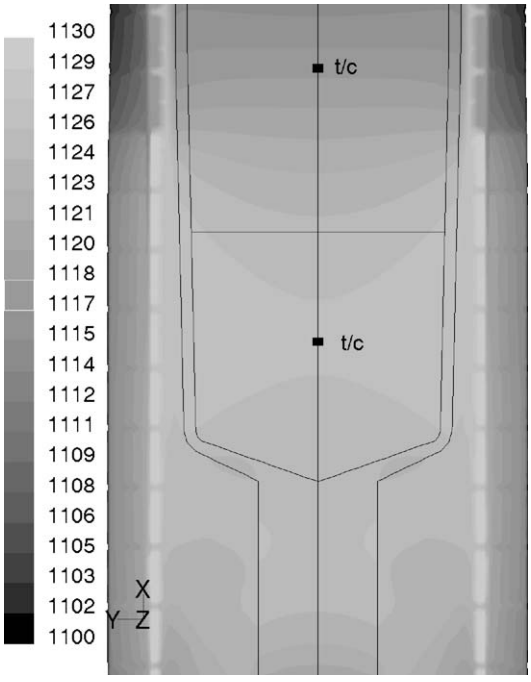

Fig. 6. Temperature profile predicted by using offsets from control thermocouples as the surface temperatures of the furnace heating elements as fixed parameters. Top thermocouple temperature was measured experimentally to be 1114 °C; the simulation value was 1116 °C. The lower thermocouple temperature was measured to be 1124 °C; the simulation value was 1126 °C.

2.5. Simulated load results

The second type of simulated growth experiments used an insert formed from "lava"—a dehydrated form of pyrophyllite (hydrous aluminum silicate). This material was used because it closely replicated the thermal properties of solid CdZnTe, and because it possessed high thermal and mechanical stability. This insert was shaped like a typical CdZnTe ingot, and had a centerline bore for a

Fig. 7. "Lava" simulated load.

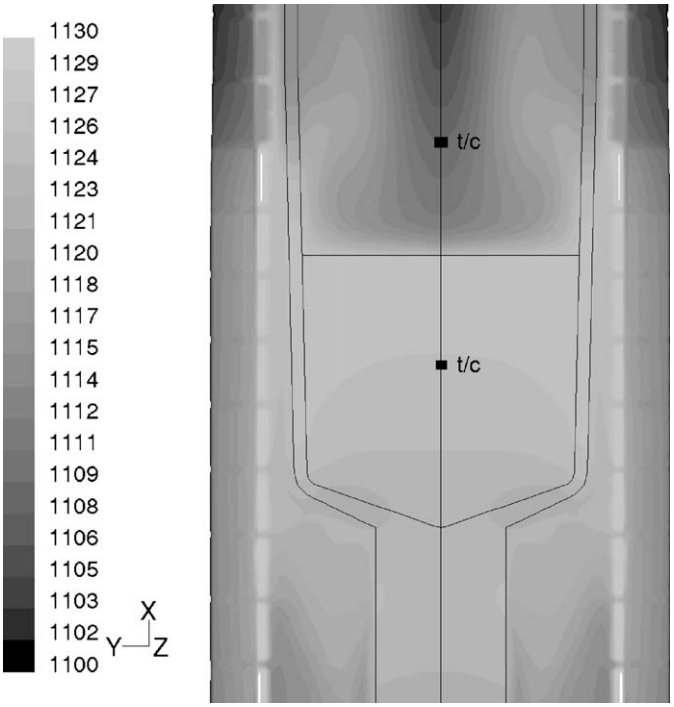

Fig. 8. Temperature profile predicted by model for lava-simulated load. Top thermocouple temperature was measured experimentally to be 1108 °C; the simulation temperature is 1108 °C. The lower thermocouple temperature was measured to be 1124 °C; the simulation value was 1126 °C.

thermocouple channel (Fig. 7). Thermocouples were located at 76 and 203 mm from the bottom of the crucible, which put the topmost thermocouple in the vapor space inside the crucible and the lower thermocouple well-centered inside the body of the insert. In this way, the effect of the argon-filled head space inside the crucible upon the heat transport of the furnace can be evaluated and quantified. In turn, this measurement can be quantitatively compared with that occurring for a real load, in which the melt affects the heat transport due to internal convection and its transparency to radiation.

The simulation and experiment agreed to within 2 °C (Fig. 8). This result validated the free convection aspect of the model, which lead to the conclusion that the heat transfer within the Gen-3 HP-EDG model is accurately described. Radiation, conduction, and convection—the three modes of heat transfer present within the furnace—were all modeled properly, and the steady-state physical properties affecting the heat transfer were sufficiently accurate to begin higher-level modeling of phenomena such as solidification and solid solution composition changes.

2.6. Turbulence

Turbulence is an unsteady and irregular flow in which transported quantities (mass, momentum, temperature) fluctuate in time and space. A worthwhile calculation of the importance on turbulence upon heat transfer is the dimensionless Raleigh number, which is the product of the Grashof number and the Prandtl number:

$$\mathrm{Ra} = \frac{\beta g \rho^2}{\mu^2} L^3 \Delta T \times Pr, \tag{7}$$

where β is the thermal expansion coefficient (constant for an incompressible ideal gas), L is a characteristic dimension, and Pr is the Prandtl number of the fluid (~0.7 for most gases). For the Gen-3 HP-EDG furnace, this yields a Raleigh number of $\sim 10^9$, which is approximately the region where turbulence can become important to the heat transfer. The direct practical application of the importance of turbulence lies in the sizing of power elements such as transformers and silicon-controlled rectifiers, which become more expensive with increased power requirements. Since the heat transfer across the boundary layer of a turbulent fluid is greater than that of a laminar fluid [10], ignoring the possibility of turbulence could be costly indeed.

Turbulence is modeled by using a Reynolds-averaged approach in which the scalar or scalar part of a vector quantity is used, and a statistical measurement of the variation about this average is supplied to the model. This perturbation theory is applied to the Navier–Stokes equations in all dimensions [10]:

$$\frac{D\vec{v}}{Dt} = \vec{g} - \frac{\nabla P}{\rho} + v\nabla^2\vec{v}, \tag{8}$$

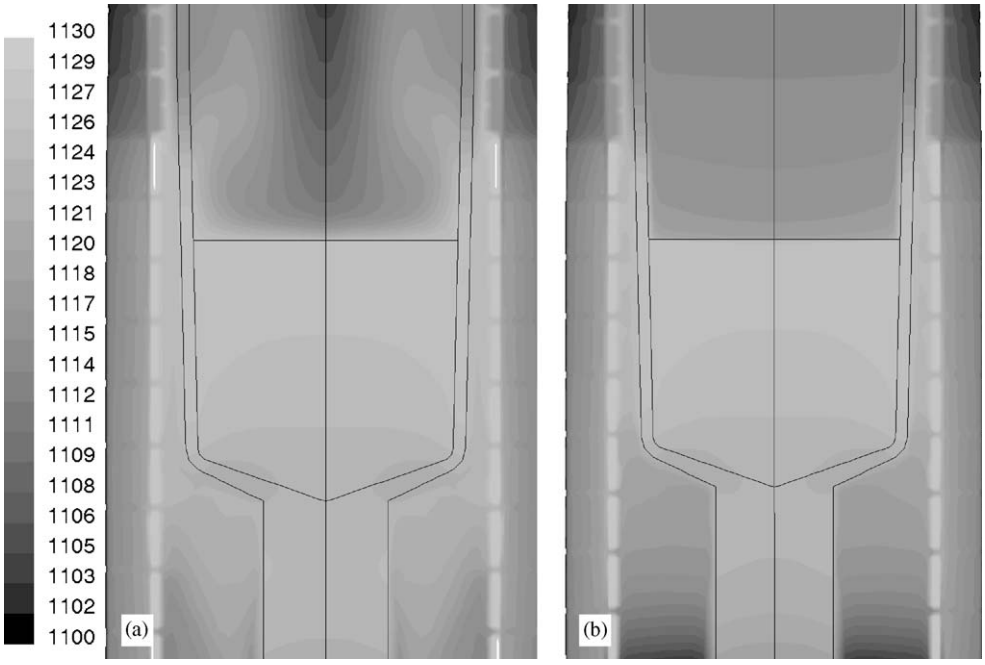

Fig. 9. (a) Temperature profile predicted by the laminar solver, for the lava insert. Top thermocouple temperature is 1108 °C, matching the experimental results. (b) Temperature profile predicted using the $k-\varepsilon$ turbulence model. Top thermocouple temperature is 1115 °C. Note that the temperature distribution in the lava insert is very similar in each case.

where $\vec{g}$ is the gravity vector, P the pressure, and v the kinematic viscosity μ/ρ.

From these, two separate transport equations for the turbulent velocity (average) and length scales (deviation) are applied and solved. For this study, the effect of turbulence was simulated by relaxing the model to permit turbulence in all fluid domains, and to use the Standard k–ε model, which is a simple yet complete model.

The effect seen was minimal, as shown in Fig. 9. Power consumption increased by less than 0.1%, and the temperature isotherms were very similar in both laminar and turbulent cases. The primary effect was a reduction in the gas-phase velocities around the heater elements (not shown), and an increase in temperature of the vapor. This may affect subsequent modeling of species transport (for instance, Cd vapor), but is not consequential at this level of solidification model development. However, since the laminar model most accurately represented the vapor space temperature measured by experiment, turbulence should be ignored for this treatment.

3. Conclusions

A descriptive computational model was developed for an advanced HP–EDG furnace, and validated through a series of steady-state experiments. Two- and three-dimensional meshes were used to model heat transfer by radiation, convection, and conduction. The results of the final model represented the experimental temperature measurements to within 2 °C, and exactly replicated the gradient between measurements. Within the model framework, a sufficiency of physical parameters and boundary conditions were validated as either being substantially correct, or relatively insignificant for the determination of the temperature field. By contrast, the local temperature gradient surrounding the control thermocouple was found to be critical to the accuracy of the model. Finally, the effect of modeling the turbulence in the high-pressure, high-temperature regime was found to be minimal in comparison to the laminar case, despite a Raleigh number analysis that suggested that turbulence was not insignificant. The small effect of a slightly increased temperature in the vapor space above the melt was discredited by comparison with experimental values. No major effect upon the vapor head velocity or temperature distribution was found.

Several aspects of the model validation continue. The most important of these are integrating a species transport capability into the model and testing it, validating the solidification module by investigating the predictions of the interface shape, and continuing to clarify the unsteady-state behavior of the HP–EDG furnaces. Additionally, the use of FLUENT as a tool for the design of experiments continues. Serial and parallel modifications to the furnace and the crucible geometry are being investigated, as well as heat transport issues and advanced control strategies. As the capabilities of the CFD model are explored, expanded, and validated, its value as a predictive tool increases. Since full-scale crystal growth experiments require several thousand dollars to run, and consume a month (or more) of valuable furnace production time, predictive virtual models enable cost-effective simulation for system and process development. Although this design capability has

heretofore been modest, it will increase as the more esoteric and complex features of the model are validated.

Acknowledgements

The authors are indebted to J.-O. Ndap, W. C. Chalmers, T. Kloes, K. Echard, and G. Rankin for their assistance with the experiments. Furthermore, invaluable discussions took place with J.-O. Ndap, T. Kloes, T. Rule, W. Wangard, and B. Devulapalli. This work has been supported in part by Defense Threat Reduction Agency (DTRA) under Contract #DTRA01-03-0035.

References

[1] K. Lin, S. Boschert, P. Dold, K.W. Benz, O. Kriessl, A. Schmidt, K.G. Siebert, G. Dziuk, J. Crystal Growth 237–239 (2002) 1736.
[2] X. Liu, W. Jie, Y. Zhou, J. Crystal Growth 219 (2000) 22.
[3] S. Kuppurao, S. Brandon, J.J. Derby, J. Crystal Growth 158 (1996) 459.
[4] C. Martinez-Tomas, V. Munoz, J. Crystal Growth 222 (2001) 435.
[5] A. Yeckel, F.P. Doty, J.J. Derby, J. Crystal Growth 203 (1999) 87.
[6] Fluent 6.1 User Manual, Fluent, Inc., Lebanon, NH, 2005.
[7] D.R. Lide (Editor-in-Chief), CRC Handbook of Chemistry and Physics, 82nd ed., CRC Press, Cleveland, OH, 2002.
[8] M. D. Reed, Cs. Szeles, in: Thirteenth International Workshop on Room-Temperature Semiconductor X- and Gamma-Ray Detectors, Portland, OR, 2003.
[9] Cs. Szeles, S.E. Cameron, S. Soldner, J.-O. Ndap, M.D. Reed, J. Electron. Mater. 33 (2004) 742.
[10] J.R. Welty, C.E. Wicks, R.E. Wilson, Fundamentals of Momentum, Heat, and Mass Transfer, third ed, Wiley, New York, 1984, p. 152.